

Tidal Downsizing Model. IV. Destructive feedback in planets.

Sergei Nayakshin¹

¹*Department of Physics and Astronomy, University of Leicester, Leicester LE1 7RH, UK. E-mail: sn85@le.ac.uk*

Accepted XXX. Received YYY; in original form ZZZ

ABSTRACT

I argue that feedback is as important to formation of planets as it is to formation of stars and galaxies. Energy released by massive solid cores puffs up pre-collapse gas giant planets, making them vulnerable to tidal disruptions by their host stars. I find that feedback is the ultimate reason for some of the most robust properties of the observed exoplanet populations: the rarity of gas giants at all separations from ~ 0.1 to ~ 100 AU, the abundance of $\sim 10 M_{\oplus}$ cores but dearth of planets more massive than $\sim 20 M_{\oplus}$. Feedback effects can also explain (i) rapid assembly of massive cores at large separations as needed for Uranus, Neptune and the suspected HL Tau planets; (ii) the small core in Jupiter yet large cores in Uranus and Neptune; (iii) the existence of rare “metal monster” planets such as CoRoT-20b, a gas giant made of heavy elements by up to $\sim 50\%$.

1 INTRODUCTION

From a single star to a cluster of galaxies, large self-gravitating astrophysical systems are similar in two ways. Firstly, gravitational collapse is the first step towards formation of these systems (e.g., see Larson 1969; Sunyaev & Zeldovich 1972; White & Rees 1978; Fall & Rees 1985, for formation of stars, galaxies and globular clusters). Secondly, most of these systems suffer from energetic feedback released by very compact sub-parts of the systems. For example, red giants are stars which experience a sudden increase in the rate of nuclear reactions in or near the core. They swell by up to ~ 100 times and eventually loose (e.g., Vassiliadis & Wood 1993) most of their envelope, leaving behind very dense cores composed of heavy elements, the white dwarfs. Negative feedback is also important during formation of stars and star clusters (e.g., Krumholz et al. 2009; Dale & Bonnell 2008). Similarly, galaxies, including our own, miss a significant amount of primordial gas believed to have been expelled by energetic feedback (Cen & Ostriker 1999) due to stars (e.g., Agertz et al. 2013) and super-massive black holes (King & Pounds 2015).

Core Accretion (CA), the de-facto accepted theory for planet formation, (Safronov 1972; Pollack et al. 1996; Ida & Lin 2004; Mordasini et al. 2009), excludes planets from this universal behaviour: planets grow bottom-up, and there is no scope for feedback. The first step in CA is assembly of $\sim 1 - 100$ km sized rocky or icy bodies called planetesimals (for a recent review see, e.g., Johansen et al. 2014). These bodies coagulate to form planetary mass solid cores (Hayashi et al. 1985), which then attract massive gas atmospheres from the surrounding disc. The atmospheres collapse and promote further gas accretion onto the massive cores (Mizuno 1980; Stevenson 1982; Hubickyj et al. 2005). This

eventually culminates in making gas giant planets. Massive cores are hence cradles of all types of planets in CA.

In this paper I argue for the opposite point of view in the context of the recently developed Tidal Downsizing (TD) theory for planet formation (Boley et al. 2010; Nayakshin 2010a):

- (I) All planets begin forming by gravitational collapse of gas-dominated fragments;
- (II) Massive cores are the sources of energetic feedback, and are the main reason why so few gas giants exist.

Point (I) has been discussed previously. In TD, Gravitational Instability (GI) of cold massive protoplanetary disc hatches gas fragments at distances of tens to hundreds of AU from the host star (Kuiper 1951; Boss 1997; Rice et al. 2005; Helled et al. 2014). As fragments migrate towards the host (e.g., Baruteau et al. 2011; Michael et al. 2011; Tsukamoto et al. 2015), massive solid cores are assembled inside them by grain sedimentation (Helled et al. 2008; Nayakshin 2011b). Fragments that are disrupted by tidal forces from the host stars leave their rocky cores behind, which are, by large, fully made planets with mass from sub-Earth to many times larger (e.g., Boley et al. 2010; Nayakshin 2011b). Fragments that managed to stay intact mature into jovian gas planets. Recent population synthesis calculations (Nayakshin & Fletcher 2015) found that many of the observed properties of exoplanet populations, previously claimed to be only accountable with CA, e.g., the positive correlation of gas giant planets with metallicity of the host stars (Fischer & Valenti 2005; Ida & Lin 2004; Mordasini et al. 2009), over-abundance of metals in planets compared to the host stars (e.g., Miller & Fortney 2011), planet mass function, etc., are also naturally explained by TD.

The main focus of this paper is point (II), that is, the role played by feedback in TD. I perform numerical coupled protoplanetary disc evolution – planet formation calculations very similar in set-up to those of [Nayakshin & Fletcher \(2015\)](#), but with three varying assumptions about core formation and their luminosity output. The “standard” simulation is nearly identical to those in the quoted paper but uses somewhat relaxed grain sedimentation assumptions, promoting faster core growth. The second simulation is identical to the first but the luminosity of the cores is set to be 10^5 times lower, rendering core’s feedback unimportant. Finally, in the simulation “no cores” core formation is turned off, which makes it similar to those in [Nayakshin \(2015c\)](#), where no core formation was allowed, although with more disc physics included here.

I find that without core formation, or with core formation but with their energy release artificially suppressed, TD is unable to account for a number of observational facts, such as the observed planet and core mass functions, constraints from direct imaging surveys on the frequency of gas giants at large separations, existence of large scale debris discs, etc.

With the energy release by the core included in the models, planet’s evolution takes two divergent paths depending on the luminosity (mass) of the core. If core’s mass is below \sim a few M_{\oplus} , the core is unimportant for the fragment, and it is pretty much a passive passenger of the fragment. However, if and when the core’s mass exceeds $\sim 5 M_{\oplus}$, its energy release starts to affect the host gas fragment by slowing down its contraction and even reversing it into expansion. This leads to most of fragments with cores more massive than a Super Earth being tidally disrupted.

This result has a number of attractive observational implications:

(1) Super-Earth to Neptune mass planets are made in very frequent gas fragment disruptions, so they are the most common type of planets ([Mayor et al. 2011](#); [Batalha et al. 2013](#)).

(2) The mass of $\sim 10 - 20 M_{\oplus}$ forms the barrier above which most solid cores cannot grow or else they destroy the parent fragment. The planet and core mass functions predicted by TD scenario both nose-dive above these masses, as observed ([Mayor et al. 2011](#); [Howard et al. 2012](#)).

(3) Massive gas giants in separations of $10 - 100$ AU are rare in direct imaging surveys (e.g., [Biller et al. 2013](#); [Bowler et al. 2015](#)). This is usually interpreted as evidence that massive cold protoplanetary discs do not make gas fragments by GI frequently (e.g., [Rice et al. 2015](#)). However, I find here that with introduction of feedback many of the gas giants that would have been otherwise observable in such surveys get disrupted, leaving behind Super Earth to \lesssim Saturn mass planets, which are not directly observable yet.

(4) The disruption remnants are produced rapidly (in under 1 Myr), which is a bonus since it may explain formation of planets with properties consistent with Uranus and Neptune in the Solar System and the suspected HL Tau planets. In §6.4 I detail arguments why TD scenario for making HL Tau appears to be much preferable to anything that can be offered by CA or GI scenarios;

(5) Although discussed in a separate paper (Fletcher & Nayakshin 2015, to be submitted), same disruptions yield debris rings with radii from a few to over 100 AU (see also

[Nayakshin & Cha 2012](#)). These debris discs have metallicity correlation properties consistent with observations.

(6) The largest giant planet in the Solar System, Jupiter, appears to have the smallest core ([Guillot 2005](#)). This is peculiar in the context of CA but is natural in the view of results presented below. Neptune and Uranus cores grew too large, and hence their Hydrogen envelopes were expelled due to the intense feedback from their cores (this was suggested already by [Handbury & Williams 1975](#)). Jupiter avoided this fate because its core is far less massive;

(7) It turns out that for a small number of fragments, pebble accretion onto the fragment and the core grain growth rate adjust to one another, and hence the fragment can accrete grains without being disrupted for a long time. This creates particularly metal-rich planets, with metallicities up to $Z_{\text{pl}} \sim 0.4 - 0.5$. I propose this scenario for formation of the “metal monster” gas giant CoRoT-20b ([Deleuil et al. 2012](#)).

I therefore suggest that negative feedback from massive cores during formation phase of planets is a key process that deserves a correspondingly important place in theory of planet formation.

Section 2 presents analytical arguments explaining why feedback from massive cores ought to be important for pre-collapse gas giant planets, and derives the critical core mass, M_{sd} , at which a fragment would self-disrupt. In §3.1, an isolated planet case, fed by pebbles at a high rate, is simulated with a radiative hydrodynamics approach, confirming the analytical suggestions. I then go on to discuss numerical methods to study the coupled planet-disc evolution in §3.2 and show an example protoplanetary disc – fragment calculation in which the fragment is disrupted due to feedback. §4 introduces the population synthesis model that is used to study planet formation outcomes of the model in a statistical sense. In §5, results of the simulations are discussed in detail. Finally, §6 considers observational implications of this paper’s results.

2 ANALYTICAL ARGUMENTS

Newly made GI fragments have virial temperatures in hundreds of Kelvin, when Hydrogen is molecular, and gas densities ~ 10 orders of magnitude lower than the density of present day Jupiter ([Bodenheimer 1974](#); [Helled et al. 2008](#); [Nayakshin 2010b](#)). Depending on fragment mass and dust opacity (e.g., [Helled & Bodenheimer 2011](#)), it takes them ~ 1 Million years to contract and collapse by H_2 molecule dissociation into the “hot start” stage usually taken as the beginning of a GI planet’s life (e.g., [Marley et al. 2007](#)). The cool and extended stage of GI fragment evolution is logically called the pre-collapse stage. To become a hot jupiter, the fragment needs to collapse or else it is disrupted, typically at a few AU distance from the star ([Nayakshin 2010a](#)).

The low temperature of pre-collapse fragments implies that very little energy is needed to unbind them: per unit mass, this energy is 4-6 orders of magnitude smaller than that needed to unbind a galaxy. The latter can only be affected significantly by energy produced by nuclear reactions in stars or by black hole accretion. We shall see now that accretion energy of a massive core is all that is needed to unbind pre-collapse gas giants.

The total energy of the fragment (pre-collapse planet)

of mass M_p and radius R_p can be estimated as that of a polytropic sphere with index $n = 5/2$:

$$E_{\text{tot}} = -\frac{3-n}{5-n} \frac{GM_p^2}{R_p} \approx -2 \times 10^{40} \text{ erg } T_3 \left(\frac{M_p}{1 M_J} \right), \quad (1)$$

where $T_3 = T_c/(1000 \text{ K})$ is the central temperature of the planet. The gravitational potential energy of a dense core of mass M_{core} , modelled as a sphere of a uniform density ρ_0 (in g/cm^3) and radius R_{core} , is $E_{\text{core}} \sim GM_{\text{core}}^2/(2R_{\text{core}}) \approx 5 \times 10^{40} (M_{\text{core}}/10 M_{\oplus})^{5/3} \rho_0^{1/3}$ erg. When the core cools, this energy is released and enters the gas envelope surrounding it (the fragment). If the fragment is unable to radiate this input energy quickly enough into the surrounding space, then it will be unbound provided $E_{\text{core}} > |E_{\text{tot}}|$. This condition can be used to set the maximum ‘‘self-disruption’’ mass of the core:

$$M_{\text{sd}} = 5.8 M_{\oplus} \left(\frac{T_3 M_p}{1 M_J} \right)^{3/5} \rho_0^{-1/5}. \quad (2)$$

We shall see that this is a robust limit for our models, and that in practice cores can hardly exceed mass of $\sim 20 M_{\oplus}$. This results be anticipated as following. The fragment’s central temperature, T_c , cannot exceed $\sim 2,000$ Kelvin or the fragment would collapse through H_2 dissociation (e.g., Bodenheimer 1974); hence, $T_3 \lesssim 2$. The core cannot grow by grain sedimentation in post-collapse fragments, of course, since even most refractive grain species vaporise above temperature $\sim 1500 \text{ K}$ (see Nayakshin 2014, for detailed description of grain physics used here). Further, most massive cores are actually assembled in moderately massive fragments, $M_p \lesssim$ a few Jupiter masses (see fig. 18 in Nayakshin & Fletcher 2015) since fragments of higher masses contract more rapidly, becoming too hot for grain sedimentation, and making *smaller* cores than their less massive counterparts (see Helled & Schubert 2008; Nayakshin 2011b). For example, a fragment of $4 M_J$ contracts radiatively $\sim 10^3$ times more rapidly than a fragment of mass $0.5 M_J$ (e.g., see fig. 1 in Nayakshin 2015b). Addition of pebble accretion accelerates this collapse even further. Therefore, the factor in brackets in equation 2 does not exceed ~ 6 or so.

Making parallels to other astrophysical objects, equation 2 is akin the so-called $M\text{-}\sigma$ limit for super-massive black holes; black holes more massive than that expel the gas from the parent galaxy (e.g., Silk & Rees 1998; King 2003). One may hence expect that the mass of $\sim 10 M_{\oplus}$ will stand out as an important feature in the observed planet populations.

3 CALCULATIONS

I use two computational methods to check analytical predictions. In the first, an explicit 1D radiative hydrodynamics (RHD) code is used to model the planet only. The second (§3.2) simplifies the treatment of the planet by assuming a hydrostatic balance and a fully convective structure for the planet, but also includes a time-dependent model for the disc and the planet-disc interaction. The first approach is more accurate as far as the planet evolution is concerned but is unfortunately too slow due to its explicit nature, the second is less accurate for the planet’s internal variables but

is more numerically expedient and can be applied to study statistical outcomes of feedback for planet formation.

3.1 A stand-alone planet calculation

I start with the simplest numerical setup: an isolated planet of a fixed gas mass that accretes pebbles at a specified rate, \dot{M}_z . The rate is prescribed via time scale t_z :

$$\dot{M}_z \equiv \frac{Z_{\odot} M_p(0)}{t_z}, \quad (3)$$

where $Z_{\odot} = 0.015$ is Solar metallicity (Lodders 2003), and $M_p(0)$ is the initial total mass of the planet. In this section only, I use the same planet evolution code as that described in §3 of Nayakshin (2015b). Spherically symmetric Lagrangian hydrodynamics in 1D approximation is used to model the evolution of both gas and four grain species (water, organics, rocks and Fe). Grains are allowed to grow by sticking collisions and can get fragmented in high speed collisions or vaporised if the surrounding gas is too hot (see for more detail Nayakshin 2014). The equation of state for the gas includes H_2 molecule rotational and vibrational transitions, dissociation, and H atom ionisation. Here we use interstellar grain opacity multiplied by a factor of 0.1 to allow for grain growth, but the results are weakly dependent on opacity unless dust opacity is another order of magnitude smaller (see Nayakshin 2015a, for a discussion of the role of grain opacity in TD).

The calculation presented here is identical to similar runs presented in Nayakshin (2015b), except that core growth was turned off in the cited paper, while here it is allowed. While the gas fragment is modelled explicitly, the central core is simply set to have a fixed material density $\rho_0 = 3 \text{ g/cm}^3$. The gas fragment has two boundary conditions, one at $R = R_{\text{core}}$, the core radius, and the other at the outer radius of the planet, $R = R_p$. On the inner boundary, the luminosity is set to $L(R_{\text{in}}) = L_{\text{core}}$, the core luminosity (see §A4). The total energy of the fragment hence decreases due to radiative losses from the surface, L_{rad} , but increases due to energy injection from the core at rate L_{core} .

Finally, pebbles accreting onto the fragment add additional mass and gravitational potential energy to the fragment (see Nayakshin 2015b,c). The latter term is negative. The positive term due to the deposition of pebble’s kinetic energy into the planet is very small because the pebble’s velocity is not the free fall one as it would be if pebbles accreted onto the planet in vacuum, but is given by the sedimentation velocity in the extended atmosphere around the planet, and also cannot exceed grain breaking velocity of a few to a few tens of m/sec.

To understand the fragment’s evolution, consider the total energy conservation equation for it¹,

$$\frac{dE_{\text{tot}}}{dt} = -L_{\text{rad}} + L_{\text{core}} - L_{\text{peb}}, \quad (4)$$

where the last term is the fragment’s potential energy change

¹ This equation is not solved directly by the RHD code, but is obeyed due to energy conservation. This equation is actually used for evolving the fragment in the simpler ‘‘follow adiabats approach’’ utilised in planet-disc co-evolution experiments as detailed in §3.2.

due to the pebble accretion onto the planet at the rate $\dot{M}_z > 0$, which has dimensions of a luminosity:

$$L_{\text{peb}} = \frac{GM_p \dot{M}_z}{R_p}. \quad (5)$$

This term is negative because the potential energy gained by the fragment as pebbles are added is negative. For moderately massive gas giants, $M_p \lesssim$ a few M_J , L_{rad} is small, and pebble accretion is usually the dominant effective cooling mechanism for such fragments (Nayakshin 2015b). Clearly, when the right hand side of equation 4 is negative, the fragment contracts, and vice versa.

In the experiments shown in this section, the initial cloud mass, metallicity and central temperature are $M_p = 1M_J$, Z_\odot and 150 K, respectively. The metal loading time scale is set to $t_z = 2000$ years. Figure 1 compares two runs, one without grain growth and without core formation (so identical in setup to Nayakshin 2015b), and the other with grain growth and core formation allowed. Panel (a) of the figure shows in black colour the evolution of T_3 , the central fragment’s temperature measured in 10^3 K, and the planet’s radius, R_p [au], shown with blue curves. The solid curves show the case of the fragment with the core, whereas the dotted ones correspond to the core-less fragment. Panel (b) of fig. 1 shows the core mass, in Earth masses, and the luminosity of the core and the pebble accretion luminosity, as indicated in the legend. The units for the luminosity curves are $10^{-5}L_\odot$.

Core’s growth initially proceeds very slowly because the initial size of grains in our calculations is 10^{-2} cm, and the grains first grow mainly due to Brownian motion of smaller grains sticking to the larger grains. However, once grains reach the size of ~ 1 cm, they are able to sediment much quicker and hence core’s growth takes off at that point.

The comparison of the black and the blue curves in panel (a) shows that massive core formation reverses the fragment collapsing trend (that is, R_p decreasing while T_c increases) when the core’s luminosity exceeds L_{peb} . By the end of the calculation the fragment is completely unbound. The mass of the core reached by that point is $M_{\text{core}} = 15.2M_\oplus$, which is consistent to what is expected based on equation 2. The last episode of core growth before it gets disrupted in this simulation is due to a late burst of $1.3M_\oplus$ water ice accretion onto the core. This becomes possible when the central temperature drops low enough for water to condense out as ice. Such later water ice accretion events are never found in simulations without feedback because the fragments only heat up with time in such simulations and the fragments’ central parts are always too hot for water ice (this was first pointed out by Helled et al. 2008).

This simulation confirms that massive and luminous core formation may lead to disruption of the fragments as envisaged in the analytical argument. It is interesting to now consider the more complicated situation when pebble accretion is determined by the co-evolution of the planet and the disc. In such more complicated situation, the planet migrates in and may open a gap, while the protoplanetary disc loses mass to the star and to a photo-evaporative wind. The spectrum of outcomes is hence much richer than it is for the isolated (albeit accreting pebbles) planet that we considered in this section.

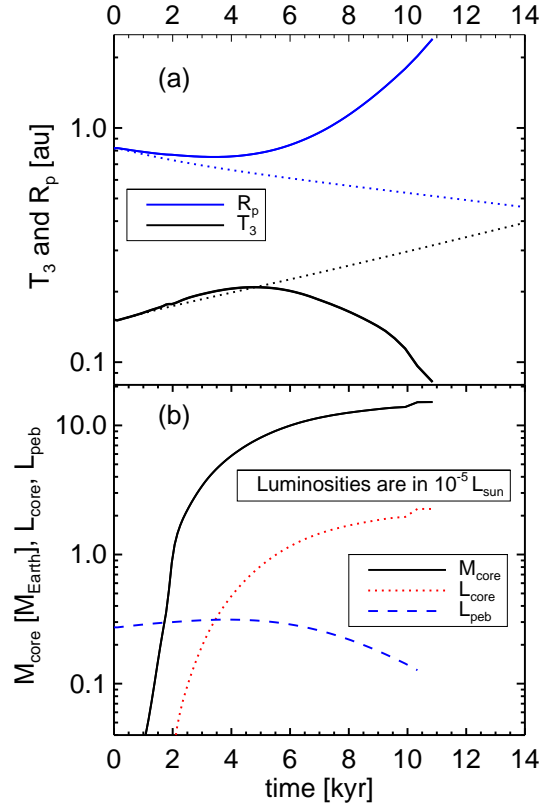


Figure 1. Panel (a) shows the gas fragment central temperature $T_3 = T_c/10^3 K$, and planet radius, R_p , versus time for simulations with (solid curves) and without (dotted) core formation, as described in §3.1. Panel (b) shows the core mass, M_{core} , core luminosity, L_{core} , and pebble luminosity, L_{peb} , for the simulation with core formation and feedback. Note that the fragment starts to expand when L_{core} exceeds L_{peb} .

3.2 Planet-disc evolution experiments

To calculate the evolution of both the protoplanetary disc and the planet, I use a 1D viscous disc plus a 1D spherically symmetric planet evolution codes coupled as described in Nayakshin (2015a) and in the appendix A. The planet evolution module is simplified in terms of gas fragment evolution compared to the method used in §3.1, which is too slow and computationally expensive to combine with a protoplanetary disc evolution code. The method used here and in the rest of the paper is to assume that the fragment is strongly convective and therefore has a uniform specific entropy. The latter changes with time, of course, as the fragment contracts or expands.

In short, a simulation begins with a gas fragment born in the outer disc at $a \sim 100$ au. Gravitational torques from the disc push the fragment in. I calculate pebble accretion rate onto the fragment, fragment’s irradiation, and internal processes, such as grain growth, sedimentation and core assembly. This determines the rate of fragment contraction and its other properties. At the same time, the disc mass decreases due to accretion onto the star and photo-evaporation. The simulation stops when the disc is dissipated away or the

fragment reaches the innermost radius of the computational domain (set at $R_{\text{in}} = 0.1$ AU here). Pebble accretion onto the gas fragment is a particularly important addition to TD framework, due to which gas fragments become metal rich, make more massive cores, and collapse faster (Nayakshin 2015b) than due to the usually considered radiative cooling alone (e.g., Bodenheimer 1974).

As with the RHD code used in §3.1, the planet evolution module of the code (see appendix A3) deals with the gas-dust part of the planet explicitly but assumes the central core to have a fixed material density $\rho_0 = 3$ g/cm³. The planet’s properties are evolved by solving the energy conservation equation 4.

Expansion of a fragment while it continues to migrate inwards tantamount to suicide since the Hill’s radius of the planet, $R_H = a(M_p/3M_*)^{1/3}$, keeps shrinking and the planet will be disrupted when it fills its Roche lobe. Since pebble accretion drives planet contraction, and since higher metallicity hosts provide higher \dot{M}_z , gas fragment survival against tidal disruption is much more likely at high metallicities. This explains (Nayakshin 2015c; Nayakshin & Fletcher 2015), in the context of TD, why gas giants at small separations are found to be almost exclusively around metal rich hosts.

To exemplify the self-destructive fragment evolution anticipated in §2, a single planet formation experiment with our defaults assumptions (picked from suite of simulations “ST”, see below) is shown in fig. 2 with thick curves. This calculation starts with a gas fragment born at $a \approx 80$ AU with initial mass of $M_p \approx 0.7 M_J$. The fragment initially contracts due to pebble accretion, but when the core feedback becomes too powerful, the fragment self-inflates, gets disrupted, and leaves behind a massive ($M_{\text{core}} \approx 12 M_{\oplus}$) core. This transformation of the fragment from a potential gas giant into a “just” a massive core occurs in only ~ 0.2 Myr, although the core stops migrating only when the disc is dissipated away.

The black, the red and the blue curves in panel (a) show the time evolution of the planet-host separation, a , Hill (R_H) and planet (R_p) radii, respectively.

The black curve in panel (b) shows the fragment’s central temperature, T_c , whereas the red and the green show L_{core} and L_{peb} , respectively. The kinks and jumps in the T_c curve are due to grains vaporising or re-forming (our equation of state takes into account the latent heat of grain vaporisation for the three grain species we consider; see Nayakshin 2014). The radiative luminosity of the fragment is much smaller than the other two dominant terms (L_{peb} and L_{core}) for this calculation. While $L_{\text{core}} \ll L_{\text{peb}}$, T_c keeps increasing with time and R_p decreases. This construction is due to pebble accretion and is similar to the core-free evolution studied in Nayakshin (2015b). However, once $L_{\text{core}} > L_{\text{peb}}$, the fragment starts to expand, and its T_c decreases. Since R_p increases as R_H decreases with time, the fragment is eventually disrupted at $t \approx 0.19$ Myrs. Having destroyed its gas envelope, the core is nearly naked: the dense atmosphere near the core (calculated as in Nayakshin et al. 2014) weighs only $M_{\text{atm}} \sim 0.3 M_{\oplus}$. The end result is a core-dominated planet, somewhat similar to but a little less massive than Neptune, at $a = 44$ AU.

Overall the planet’s evolution is this coupled planet-disc calculation is very reminiscent of the isolated planet

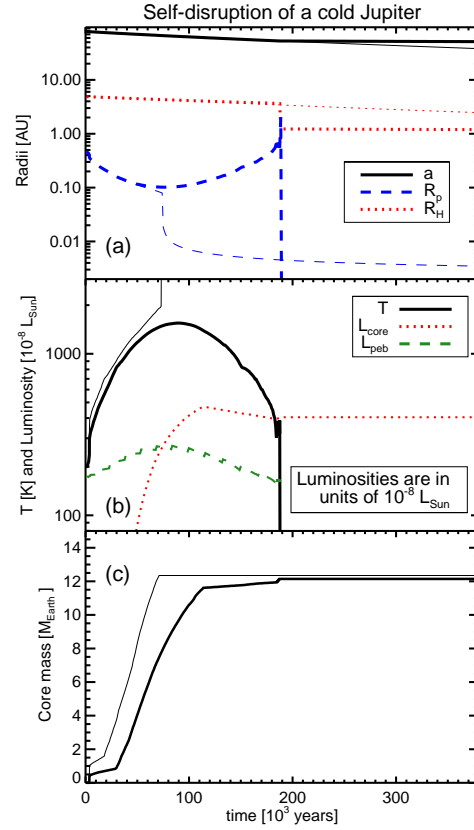


Figure 2. Thick curves: evolution of a fragment in one of the ST simulations that ends with a massive core disrupting the fragment at about 0.2 Myr. Panel (a) shows the planet-star separation (black solid), R_H and R_p , versus time; (b) shows the central temperature T_c , L_{core} and L_{peb} ; (c) shows the core’s mass. Thin curves are for an identical simulation but with L_{core} arbitrarily reduced by a factor of 100. In the latter case the fragment manages to collapse and survives as a gas giant planet at $a \approx 10.5$ AU.

run presented in §3.1, although the pebble accretion rate onto the fragment is lower, and it takes it longer to build a massive enough core to self-disrupt.

To demonstrate that the planet’s disruption is induced by the core’s high luminosity for this run, even though the mechanics of the final disruption is due to tides from the host star, this calculation was repeated but this time the core’s luminosity was arbitrarily multiplied by 0.01. Thin lines in fig. 2 show the result. The core’s luminosity is now negligible in the thermal evolution of the fragment. The fragment heats up due to pebble accretion, and collapses by H₂ dissociation to much higher densities and temperatures at time $t \approx 0.07$ Myr. Its radius drops to a few times that of Jupiter (note the thin blue dashed curve in panel a), which is now always much smaller than R_H . With the much dimmer core, the planet is never disrupted. Although not shown in fig. 2, the fragment migrates in to $a \approx 10.5$ AU by $t = 2.8$ Myr, when the protoplanetary disc dissipates away, to become a gas giant with $M_p = 0.8 M_J$ (having accreted $\sim 0.1 M_J$ of pebbles). Interestingly, the core’s mass is also around $12 M_{\oplus}$ but this core is entirely engulfed by the massive gas envelope. The core does not grow much beyond that of the original cal-

culuation because once the temperature reaches $T \gtrsim 1500$ K in the centre, all species of grains are vaporised in the centre, and the core cannot grow further by grain sedimentation (Nayakshin 2011b).

4 POPULATION SYNTHESIS

It is useful to explore how massive core feedback affects planet formation outcome in a statistical sense. To reach that goal, population synthesis approach is used, in which simulations similar to the one described in §3.2 are repeated to cover a large parameter space of possible initial conditions for the disc mass, photo-evaporation rate, fragment’s initial location, mass, etc. (see appendix A5). Each of the simulations begins with a gas fragment, with a mass randomly sampled between 0.33 and 8 M_J , born at $70 < a < 105$ AU in a massive protoplanetary disc.

Fig. 3 contrasts the final planet mass versus separation distribution for three population synthesis calculations of 3000 planet-forming experiments each. Panel (a) shows simulation NC (“no cores”) in which core formation is artificially suppressed; panel (b) shows simulation DC (“dim cores”) in which core luminosity is reduced by an arbitrary factor 10^5 compared to simulation ST (“standard”) shown in panel (c) which includes the full planet and core formation physics of TD model. The main difference of simulation ST from those presented in Nayakshin & Fletcher (2015) is in the two parameters that influence grain sedimentation. Whereas the turbulence parameter α_d was varied between 10^{-4} and 10^{-2} , here it is set at 10^{-4} (cf. Table B in appendix A5). In addition, grain breaking velocity is varied between 15 and 30 m/sec, rather than 5 – 15 m/sec range considered in Nayakshin & Fletcher (2015). These choices allow a more rapid core growth, although note that convective grain mixing remains on and affects grain sedimentation significantly.

The colours of the symbols indicate metallicities of host stars, as explained in the legend. Panel (d) shows the resulting planet mass function (PMF) for the three simulations.

As mentioned above, fragments are disrupted when planet’s radius R_p exceeds its Hills radius, R_H . This forms a tidal “exclusion zone” to the left of the thin red line in panel (a). The exclusion zone boundary depends on planet mass as $a_{\text{exc}} \propto M_p^{2/3}$. This can be deduced from a simple analytical argument. Pre-collapse gas giants have central temperatures T_c less than 2000 K. Planet’s density scales as $\rho_p \propto M/R_p^3 \propto T_c^3 M_p^{-2}$, where I used $T_c \propto M_p/R_p$, the virial temperature dependence. The planet is tidally disrupted where $\rho_p \sim M_*/(2\pi a^3)$, hence the scaling. Migration of post-collapse fragments depends on fragment’s mass, of course, and this dilutes the sharpness of the exclusion boundary somewhat.

In simulation NC, nothing is left of the disrupted fragments when their gas is re-integrated into the disc and then consumed by the star (or photo-evaporated). The few planets found inside the exclusion zone collapsed before they entered it. Their protoplanetary disc dissipated away before the planets were pushed all the way through the inner disc boundary at 0.1 AU. Most of such close-in fragments are consumed by the star, although a small number may survive as hot Jupiters and are shown left of the vertical dashed line. To enhance visibility of those, they are randomly positioned

in $\log a$ between $a = 0.03$ AU and $a = 0.09$ AU (protoplanetary discs probably have inner boundaries at varying distances from the star due to different strength of their stars’ magnetic fields, so this procedure is not entirely unreasonable). For planets outside the exclusion zone, protoplanetary discs ceased to exist before they migrated inside the zone.

Simulation NC shows, in accord with previous results (e.g., Nayakshin & Fletcher 2015), that gas giant planets populating the region inside of the few AU of the host star are mainly metal-rich. This selection is driven by pebble accretion being more vigorous at higher metallicities (Nayakshin 2015c).

In simulation DC, core formation is allowed, and hence here fragment disruption does leave a core behind. It is interesting to note that core masses usually exceed $10 M_{\oplus}$ (see panel b of fig. 3 and the red histogram in fig 5 for more detail). Core’s presence does not appear to affect gas giants that stall outside the exclusion zone (compare panels a and b) because the cores are very dim in the run DC by construction. Fragments that enter the exclusion zone before they collapse are disrupted, as in simulation NC. The legacy of disruption in run DC is not just the massive cores. Most of the massive cores hold on to the densest part of the fragment in this simulation because the core luminosity is low and hence the gas layers adjacent to the core are quite dense (Nayakshin et al. 2014; Nayakshin & Fletcher 2015). These \sim Neptune to Saturn mass planets continue to migrate through the disc, and are seen as the nearly vertical “tongue” feature touching the vertical line in panel (b).

Simulation ST (panel c), performed with our default model for core’s luminosity, shows that feedback unleashed by the cores on their host fragments leads to a qualitative change in the resulting planet population. The most frequent type of planet is now a core of a mass $M_{\text{core}} \lesssim 10 M_{\oplus}$ and these cores are found at all separations explored in this paper. Gas giants are now much rarer, again for all separations. We shall now consider results from these simulations, and especially ST, in greater detail.

5 ANALYSIS OF SIMULATION ST RESULTS

5.1 Planet mass function

Figure 4 shows the planet mass function (PMF) for the three simulations. In simulation NC, there are only gas giant planets (of course), with the minimum and maximum masses simply given by the range in the fragment mass in our initial conditions. In simulation DC, fragment disruption extends the PMF towards smaller planet masses, but this extension does not go to masses lower than $\sim 10 M_{\oplus}$ because the cores are massive and are always surrounded by massive remnant atmospheres. The PMF of simulation ST that includes massive core feedback at the appropriate level is drastically different. The cores of mass $\sim 10 M_{\oplus}$ are now the most abundant planets, with very few gas giants surviving. Although disruption of gas fragments always occurs by the means of tides from the stars, comparison of runs DC and ST clearly demonstrates that core’s energy output enhances the frequency of fragment disruption significantly. The dominance of massive cores in the PMF of the TD theory is therefore in big part due to feedback released by the cores.

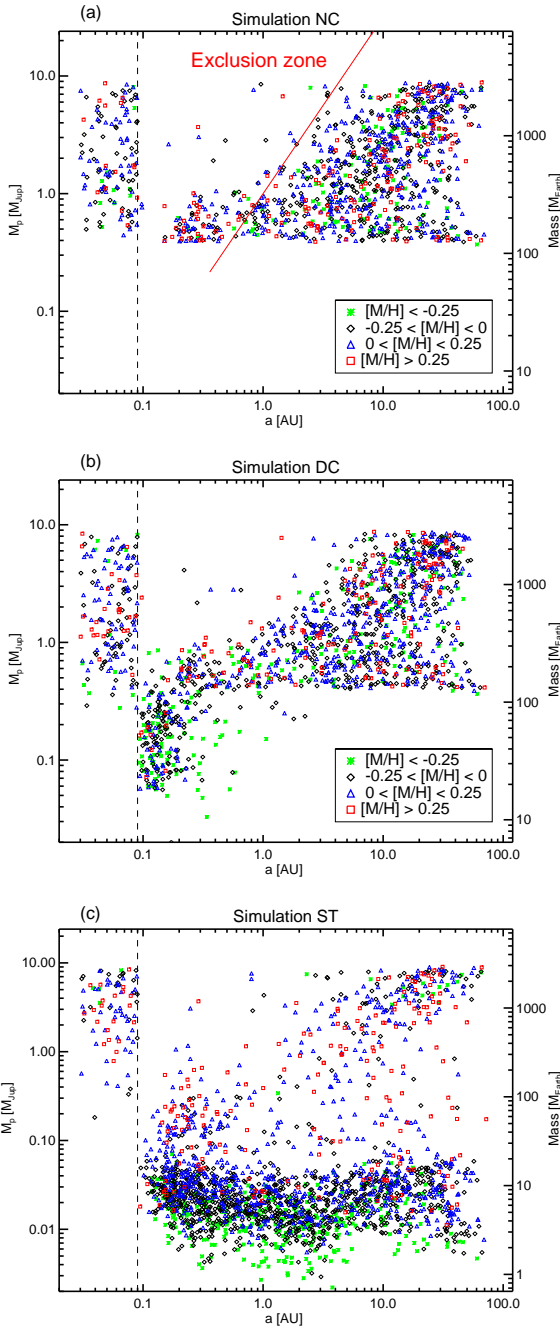


Figure 3. Final planet mass versus planet-host separation for simulations: NC (no core formation), DC (“dim cores”), and full core growth physics, ST (“standard”). Host star metallicities are colour coded). Note that cores destroy *most* of far-out giants that would otherwise survive.

5.2 Core mass function

Fig. 5 shows just the core mass function (CMF) for the simulations DC and ST (simulation NC has no cores at all by design, so it is not shown in the figure). Further, we divided the core population into those surrounded by a massive gas atmosphere, defined as being more massive than $0.2M_{\text{core}}$, and those with less massive atmospheres (“naked” cores). The hatched histogram in fig. 5 shows the popula-

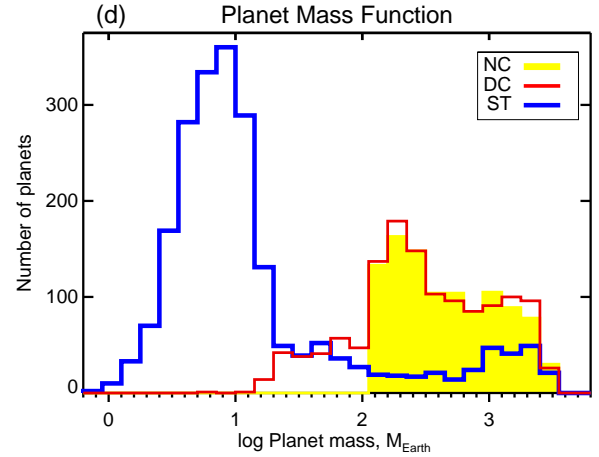


Figure 4. The planet mass function (PMF) for the three population synthesis models shown in fig. 3

tion of the naked cores in simulation ST, while the thick solid blue line shows the histogram for all cores in the same run, with or without massive atmospheres. It is clear from these histograms that in simulation ST most of the cores have small atmospheres. The smallest mass cores ($M_{\text{core}} \lesssim$ a few M_{\oplus}) have virtually no atmosphere, but for higher masses the fraction of cores with atmospheres increases. This is in agreement with previous results (Nayakshin & Fletcher 2015). For simulation DC, it turns out that all of the cores retain massive atmospheres precisely because they are so dim (see Nayakshin et al. 2014), so there is no corresponding naked core population.

The CMF of simulation ST shows a precipitous drop in the number of cores that exceed $\sim 10\text{--}20 M_{\oplus}$, in accord with the mass limit given by equation 2. Comparing the CMF of the run ST with that from the run DC we see that there is no corresponding drop in the CMF when core’s luminosity is artificially suppressed. There is instead a long tail towards high masses, with the maximum mass of the core assembled in simulation DC reaching $M_{\text{core}} \approx 71 M_{\oplus}$. Furthermore, as noted above, none of these cores are bare.

We conclude that feedback unleashed by massive cores not only reduces the number of gas giants surviving the disc migration phase but also regulates the maximum mass of the solid cores, potentially explaining why there are so few cores more massive than $\sim 20 M_{\oplus}$ (Mayor et al. 2011). In §6.2 I argue that this explanation is better consistent with the data than that given by CA theory.

5.3 Cold disruptions: “deficit” of observed gas giants

A popular argument against GI model for planet formation, and by extension against TD as well, is that gas giant planets found at separations greater than 10 AU are exceedingly rare in the direct imaging surveys. Biller et al. (2013), for example, finds that no more than a few % of stars host $1\text{--}20 M_{\text{J}}$ companions with separations in the range $10\text{--}150$ AU. Rapid inward migration may be expected to remove most of such objects even if they did form at tens of AU. However, the fraction of those that survive in our population synthesis simulations *without core feedback* is still too high. In simu-

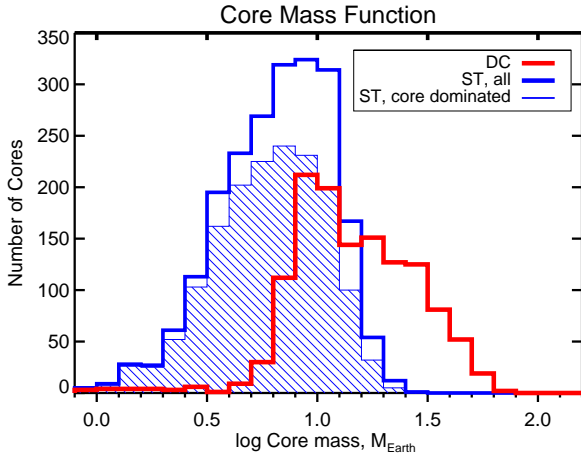


Figure 5. The core mass function (CMF) for the population synthesis models DC and ST. The thick solid curves show all cores, whereas the blue shaded histogram shows those that are naked or nearly so. Such cores are found only in simulation ST

lation DC, for example, 15.6% of the initial gas fragments survive in orbits beyond 10 AU. When the feedback is taken into account, more than two thirds of gas giants that are stranded outside the exclusion zone in simulations NC and DC are disrupted by the high luminosity cores forming inside. In simulation ST, only 4.7% of initial fragments remain at orbits wider than 10 AU by the end of the simulations. This is probably consistent with the observational limits, especially if (a) protoplanetary discs smaller than ~ 50 AU never fragmented – these stars would be planet free in the TD model, and would dilute the planet-bearing systems we discuss here; (b) companions at larger separations or close passages of other stars in star clusters eject some of the left-over giants from the systems.

Rice et al. (2015) argued that the frequency of fragment formation via disc fragmentation can be constrained by an additional argument. They find that about $\sim 5\%$ of their fragments, initially located at $a > 50$ AU, get scattered on very close orbits by distant companion stars. The authors then show that these fragments would have a very different metallicity distribution than the planets actually observed at small separations. This is clearly correct, however, Rice et al. (2015) simulations begin when the gas disc dissipates, that is roughly at the end of the simulations presented here, and concern only the clumps that are stranded on distant orbits. Most of our fragments ($\sim 95\%$ in simulation ST) have migrated due to the gas disc torques into the inner disc or have been disrupted by the feedback by that time. Hence, the frequency of occurrence of objects scattered by the secondary’s N-body torques to small separations (as calculated by Rice et al. 2015) in simulation ST would be at most about $0.05 \times 0.05 = 2.5 \times 10^{-3}$, which is too low compared with the population of planets that migrate there directly during the gas disc migration phase. Hence, Rice et al. (2015) arguments do not contradict our scenario at all.

Furthermore, disruption due to cores is especially severe for moderately massive fragments. For fragments with mass $M_p \leq 3 M_J$, for example, only 1.5% of the initial fragments survive at large separations. If only moderately massive fragments are hatched by the disc at beyond tens of AU, then

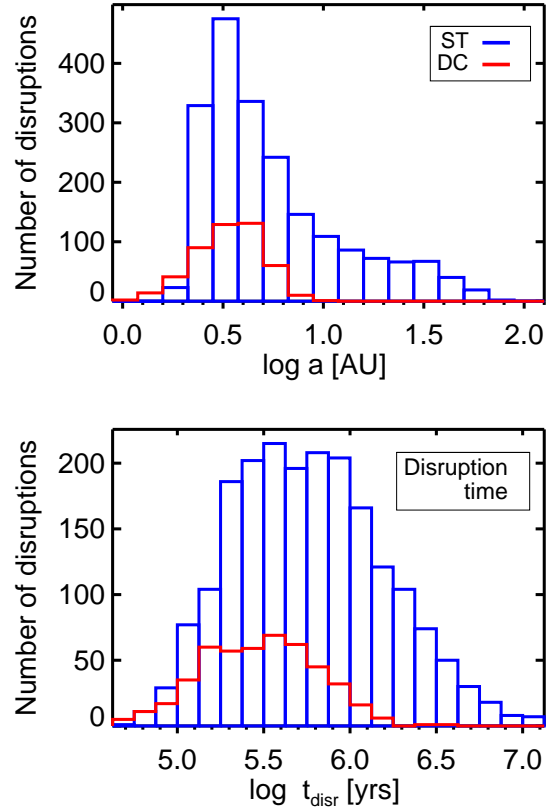


Figure 6. Top panel: host-fragment separation at the time of fragment disruption for simulations DC and ST. Bottom panel: same but for the time of fragment disruptions.

the simulation ST is consistent with the observational limits on the frequency of directly imaged gas companions *even if* several fragments are born per each disc².

TD with feedback hence predicts a significant population of cold massive solid cores, and downsized giants (\sim sub-Saturn planets) more generally, formed rapidly. Existence of such cores is an observational test of this theory, as opposed to the currently dominant view that fragmentation of self-gravitating discs is rare.

5.4 Massive and distant cores, unexpectedly young

The population of the distant young cores that must be produced when would-be-giant planets die at large separations is discussed in this section. Fig. 6 shows the locations (top panel) and the times (bottom panel) of fragment disruptions

² This is especially so since we simulate the last clump in the dispersal phase of the disc, when the disc starts to run out of mass. The clumps found beyond 10 AU in our simulations are those for which the disc was removed particularly rapidly so that they got stranded there. The earlier generations of clumps, formed in the phase of the disc when it was still accreting gas from the envelope, would never be in that regime of disc running out of mass. These early fragments are very likely to migrate in rapidly and contribute to the observed populations of close-in super-Earth planets rather than gas giants beyond 10 AU.

in simulations ST and DC. We already saw that luminous cores force many more disruptions than do “dim cores”. This is why the blue histograms contain many more disruption events than do the red ones. The top panel of fig. 6 shows that in addition to that, disruptions at large ($a > 10$ AU) separations occur only in simulation ST. This demonstrates that feedback from massive cores not only increases the number of disruptions but it also changes the conditions under which these disruptions occur.

Consulting panel (c) of fig. 3, we notice that the cold disruptions produce massive cores with mass between that of a Super Earth and Neptune, although some cores manage to hold on to more massive gas atmospheres despite the host fragment’s disruption and reach \sim Saturn mass. The bottom panel of fig. 6 shows that many of the cold disruptions occur at a young age of the system, at a fraction of a Myr. This is interestingly different from the CA theory where massive cores assembled at large distances take 10–100 Myr to grow (Kobayashi et al. 2011; Kenyon & Bromley 2015).

In sections 6.4 and 6.5, I shall argue that such cold disruptions induced by massive core feedback may offer natural explanations for assembly of Uranus, Neptune, and the suspected planets in the HL Tau protoplanetary disc.

Furthermore, here we explored the situations where the starting embryo positions are not larger than $a = 105$, a plausible but not a necessary choice. Simulations of protoplanetary discs that include its formation from larger scales show that these discs may well hatch fragments at larger radii (e.g., Vorobyov & Basu 2006; Vorobyov 2013). It therefore seems plausible that massive cores formed in TD by self-destruction of their fragments could be formed in young protoplanetary discs beyond 100 AU. In appendix B and in Fig. B2, I show an example run in which a fragment born at $a = 150$ AU self-disrupts and leaves a core of mass $M_{\text{core}} = 5.1 M_{\oplus}$ stranded at $a = 112$ AU.

5.5 Large debris discs

Not all large solids are expected to condense into the core if the fragment is rotating, which is always the case in the simulations of fragmenting gravitationally unstable protoplanetary discs (e.g., Boley et al. 2010; Nayakshin 2011a). Therefore, it is reasonable to assume that large ~ 100 km sized bodies may form inside fragments and be orbiting within it due to excess angular momentum prior to disruption. Nayakshin & Cha (2012) showed that in this case disruptions of pre-collapse fragments leave behind not only the solid cores, but also rings of smaller solids. These rings are morphologically similar to the Asteroid and the Kuiper belts in the Solar System and the debris discs elsewhere (e.g., Wyatt 2008). Such post-disruption rings of solid bodies is the TD alternative to the planetesimal discs postulated by the Core Accretion (Safronov 1972).

I defer detailed discussion of the debris disc properties formed in this model to a future publication (Fletcher & Nayakshin, in preparation). Nevertheless, it is relevant to note here the role of feedback in formation of these rings. Because feedback produced by the solid cores helps to disrupt the fragments at all radii $a > 1$ AU (top panel of fig. 6), we find debris discs of all sizes, compatible with the broad range of size in observed debris discs. Core feedback is hence

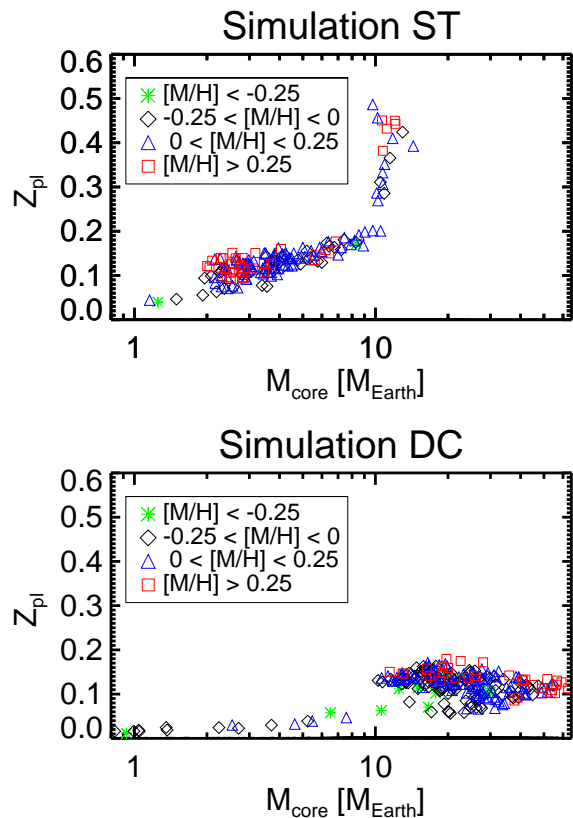


Figure 7. Internal metallicity of gas giant planets for $M_p > 1 M_J$ as the function of their core mass for simulations ST and DC. Only a subset of the planets, selected randomly, is shown for clarity.

instrumental to understanding the debris discs in the context of TD as well.

5.6 Metal Monsters

Fig. 7 plots the planet’s metallicity, $Z_{\text{pl}} = M_Z/M_{\text{pl}}$, where M_Z is the total weight of metals (elements heavier than Helium) inside a planet of mass M_p , versus the planet’s core mass for planets that were not disrupted³. The top panel shows simulation ST and the bottom one shows simulation DC. The colours of the symbols mark the four different metallicity bins, as detailed in the legend.

There is a striking difference in Z_{pl} vs M_{core} trends for the planets assembled with (simulation ST) and without (simulation DC) core feedback. The metallicities of the planets assembled without feedback first rise with M_{core} and then drop a little (the bottom panel). The rising trend at low Z_{pl} is due to metal-limited growth of cores for such low Z_{pl} : more metals implies faster grain sedimentation and a higher M_{core} .

³ These are the gas giants planets, of course. The planets less massive than \sim Saturn in TD belong to the disrupted population. These have even higher metallicities due to the presence of a massive core and their remaining gas envelopes being more metal rich than the original envelopes. See fig. 17 in Nayakshin & Fletcher (2015). To avoid these disrupted planets we include only $M_p > 1 M_J$ giants in the figure.

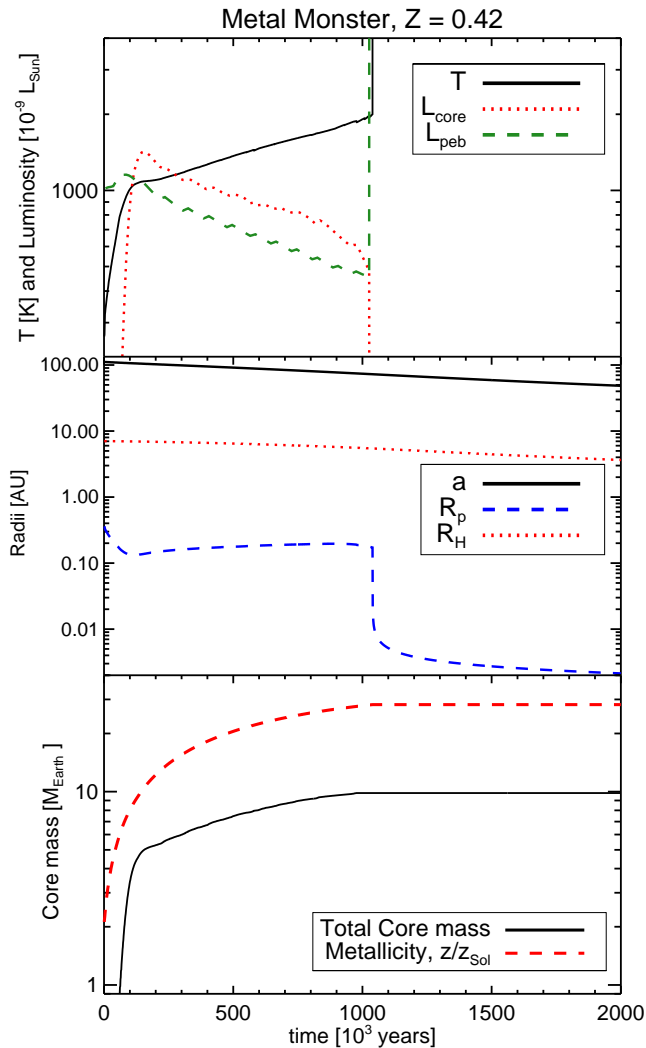


Figure 8. Similar to fig. 2. Evolution of a gas fragment versus time in a simulation that forms a metal monster planet. Note that unlike fig. 2, the core’s luminosity drops in this simulation shortly after the fragment starts to expand. This allows the fragment to hover near marginal stability while it is fed pebbles from the outside, and become very metal rich.

For most of the cores in simulation DC, planet’s metallicity is spread between 0.05 and ~ 0.15 .

Inclusion of core feedback appears to drastically change this picture. First of all, feedback self-limits mass of the cores, as explained in §5.2. This is why M_{core} values are all below $\sim 15 M_{\oplus}$ in the top panel. Furthermore, the Z_{pl} vs M_{core} relation is steeper and nearly monotonic: the higher the core mass, the higher the planet’s metal content. There is also a nearly vertical sequence of points towards surprisingly high metallicities up to $Z_{\text{pl}} \approx 0.5$, taking off at core mass $M_{\text{core}} \sim 10 M_{\oplus}$.

The results for simulations ST are best understood as a time sequence of M_{core} and Z_{pl} . Initially, as the planet accretes pebbles and the core grows, these two quantities co-evolve to larger values on parallel tracks. However, when

M_{core} reaches the mass limit $M_{\text{sd}} \sim 5\text{--}10 M_{\oplus}$ given by equation 2, its energy output starts to affect the core strongly. I find that one of the following two outcomes happen after this point.

For most of the fragments, the core luminosity continues to increase (as in panel b of fig. 2), and this puffs up the fragment. Eventually it is disrupted. This is why the cores in the top panel do not make it to higher masses, unlike the feedback-free case (bottom panel).

However, there is a small number of cases when there is a certain degree of self-limitation in the core growth, so that the fragment is not immediately disrupted. As the fragment expands, core growth rate drops because grain velocity is the sum of the (negative) sedimentation velocity and the gas (positive in this case since the fragment is expanding) velocity. In this situation the opposite terms in equation 4, L_{core} and L_{peb} , nearly balance each other and the fragment’s radius evolution stagnates despite pebble accretion. The fragment then becomes much more metal rich than expected based on the analytical model of pebble accretion by Nayakshin (2015b), in which cores were not taken into account. In that theory the fragments should collapse once $Z_{\text{pl}} \sim 0.1$ is reached, and it fits well the numerical results for the majority of planets in both panels of fig. 7.

The exceptional systems that reach much higher Z_{pl} on the vertical track exist due to core feedback. Their evolution is exemplified by fig. 8 which shows the evolution of the fragment which reached very high metallicity by the time it collapsed, $Z_{\text{pl}} = 0.42$. Focusing on the red (dotted) and the green (dashed) curves in the top panel of fig. 8, showing L_{core} and L_{peb} , respectively, we see that L_{core} indeed drops soon after the two curves intersect. This is connected to the fact that the core accretion rate dropped significantly after the feedback started to inflate the planet (as can be seen from the abrupt change in the slope of M_{core} vs time curve in the bottom panel of the figure).

I find that the fraction of gas giant planets that follow the nearly vertical evolution line in the Z_{pl} vs M_{curve} plane depends on several somewhat poorly known parameters of my numerical model, such as t_{kh} that determine the timescale on which cores release their heat of accretion, disc pebble fraction f_{p} , grain breaking velocity, v_{br} and the turbulence in the fragment, α_{d} (see appendix §A5). Therefore, the fraction of such “metal monster” gas giants cannot be yet reliably calculated, except to say that such planets should be rare, $\lesssim 10\%$.

I propose that the surprisingly high metallicity planet CoRoT-20b (Deleuil et al. 2012) formed as described in this section.

6 DISCUSSION

6.1 Main result and comparison to previous work

Here, no major changes in the TD model for planet formation were introduced compared to a recent Nayakshin & Fletcher (2015) study, except for relaxing somewhat factors controlling core growth by grain sedimentation (reducing turbulence and increasing the grain breaking velocity, see §A4 and table B). This led to a somewhat more rapid massive core assembly, and put the

effects of feedback by massive cores on their host fragments into a sharper focus. Cores more massive than $\sim 5 M_{\oplus}$ (eq. 2) affect their host gas fragments significantly by releasing enough energy to puff the fragments up. This leads to more frequent tidal disruptions of these fragments, especially at large separations from the star, and explains naturally why the TD mass and core function is strongly cut off above the mass of $\sim 20 M_{\oplus}$.

Now I discuss the most interesting observational implications of these results.

6.2 The special role of $M_{\text{core}} \sim 10 M_{\oplus}$

Small, core-dominated planets, $R_p \lesssim 4R_{\oplus}$, are very ubiquitous (Howard et al. 2012). In terms of mass, this size range translates to somewhere around $M_p \sim 20 M_{\oplus}$, above which the planet mass function (PMF) drops sharply (Mayor et al. 2011). This indicates that cores with mass $M_{\text{core}} \sim 10 M_{\oplus}$ have a special role to play in planet formation.

CA model suggest that this special role is in building massive gas giants: cores more massive than M_{crit} accrete gas rapidly (e.g., Pollack et al. 1996). However, the critical core mass can actually vary substantially depending on the planetesimal or pebble accretion rate (Stevenson 1982; Ikoma et al. 2000; Lambrechts & Johansen 2014), location in the disc (Rafikov 2006), dust opacity (Ikoma et al. 2000), and the metallicity of the atmosphere (Hori & Ikoma 2011). The range here is from a few M_{\oplus} to $\sim 50 M_{\oplus}$. It is not obvious that such a broad range of critical core masses can yield as sharp a cutoff in the PMF as observed. Furthermore, if cores that grow more massive than $10 - 20 M_{\oplus}$ rapidly become giant planets by gas accretion, when where are⁴ these giants? This scenario would predict roughly ~ 10 times more gas giants than observed (cf. the relative numbers of planets discussed in the next section), given the ubiquity of massive cores.

The explanation advanced in this paper for the special place of $M_{\text{core}} \sim 10 M_{\oplus}$ cores in planet formation paints the cores not as nurseries of gas giant planets but as sources of powerful feedback that leads to self-destruction of most gas fragments. This negative role of cores is consistent with that played by densest parts of all larger astrophysical systems. Stars, giant molecular clouds, star clusters, and galaxies all loose mass because of energy released in the densest parts of these systems.

The critical core mass derived here (eq. 2) does not depend strongly on the host star or fragment metallicities, or the distance to the host star, and does not seem to contradict any constraints from the observations of exoplanets at close separations. It appears both more robust and more logical than the one offered by the CA scenario.

6.3 The rarity of gas giant planets

Gas giant planets are very rare compared to core-dominated planets (those from Earth mass to \sim Neptune mass). In a recent very careful analysis of *Kepler*-detected giant planet candidates, Santerne et al (2015, submitted) have shown

that more than 50% are false positives, such as eclipsing binaries. This corrects downward the giant count, so that the overall frequency of gas giant planets with orbital period less than 400 days is estimated to be only $4.6 \pm 0.6\%$. This is over 10 times less frequent than planets with radii between 1 and $4R_{\oplus}$ (Silburt et al. 2015). In TD, this result is not surprising giving that most migrating gas fragments are disrupted and leave behind a massive core.

In addition, directly imaged surveys conclude that $M_p > 1 M_J$ planets are hosted by no more than a few % of nearby stars (Biller et al. 2013; Bowler et al. 2015). This is thought to indicate that gas disc fragmentation at \gtrsim tens of AU is exceedingly rare (Rice et al. 2015). However, these observations do not directly tell us the number of gas fragments born by GI in the outer disc; they only constrain the fraction of giants that survive to the present day. Migration of planets to closer separations was found to take as little as $\sim 10^4$ years in numerical simulations by numerous authors (e.g., Vorobyov & Basu 2006; Boley et al. 2010; Baruteau et al. 2011; Cha & Nayakshin 2011; Michael et al. 2011; Machida et al. 2011).

Further, here it was shown that disruption of fragments by feedback from massive cores also destroys many of the would-be giant planets. In §5.3 I showed that TD with feedback is at least qualitatively consistent with the low observed frequency of gas giant planets in directly imaged surveys (Biller et al. 2013; Bowler et al. 2015).

In detail, however, I find that theoretical predictions on number of giants stranded at large separations depend sensitively on the mass function of gas fragments born in the outer disc. Fragments more massive than $\sim 4 - 5 M_J$ are unlikely to make massive cores and hence they are not likely to be tidally disrupted. If fragment mass function is "bottom-heavy", with most fragments at $\sim 1 M_J$, then observational constraints appear to be easily satisfied; however, if most fragments were more massive than a few M_J then the model would probably over-produce "cold" giants (this can be qualitatively deduced from fig. 3c). More work, e.g., 3D simulations to understand fragment formation and their typical properties better, is needed for a quantitative comparison of TD theory with data at large separations.

6.4 The "impossible" planets in HL Tau

Gas fragment disruption by massive cores leaves the perpetrators behind. These cores can sometimes be observable. I argue that one such case may be the dust-depleted rings in HL Tau, and the other are the outer Solar System (§6.5).

HL Tau is a young ($\sim 1 - 2$ Myr old) star located ~ 140 pc away from the Sun and is the brightest protoplanetary disc in millimetre radio emission (Andrews & Williams 2005). Atacama Large Millimetre/Submillimetre Array (ALMA) has recently observed HL Tau and produced the first ever *picture* of planet formation disc. The image of HL Tau shows a number of circular depressions in the dust emissivity of the disc. Dipierro et al. (2015) reproduces the observed ALMA image in tantalising detail by having three planets with mass between ~ 0.2 to $\sim 0.5 M_J$, orbiting the star at $a = 13, 32$ and 69 AU, respectively. The planets affect the surrounding gas disc weakly, but force mm-sized grains (to which ALMA is sensitive) away from their orbits, producing the observed dark rings.

⁴ The author thanks Vardan Adibekyan for raising this question.

The actual masses of planets in HL Tau may be lower than the \sim Saturn masses inferred by [Dipierro et al. \(2015\)](#). As shown by [Baruteau et al. \(2011\)](#), Saturn or higher mass planets migrate through an outer self-gravitating disc in ~ 0.03 Myr or less. This is consistent with many other studies ([Boley et al. 2010](#); [Cha & Nayakshin 2011](#); [Michael et al. 2011](#)). The planet migration time scales as $t_{\text{migr}} \propto M_{\text{p}}^{-1}$ in the type I regime. Hence the planets of Neptune mass would migrate \sim an order of magnitude slower, and would be more likely to have been detected by ALMA.

Additionally, at least in the Core Accretion theory, planets as massive as $\sim 0.2 M_{\text{J}}$ should be accreting gas very rapidly in the HL Tau rings because the observed gaps are in the dust grains not in the gas ([Dipierro et al. 2015](#)); gas surrounds the planets. Mass doubling time for the parameters appropriate for HL Tau disc can be estimated at \sim a few $\times 10^4$ years. These planets should run away in mass into \gtrsim Jupiter mass planets. Gas accretion onto the planet should make the planets bright enough to have been detected by ALMA as brighter spots in the rings.

HL Tau planets properties are also inconsistent with the simplest, that is migration-free, variant of the Gravitational Instability model (e.g., [Boss 1997](#)). The planets are too close-in (especially the one at $a \approx 13$ AU), and are too low mass. The minimum (Jeans) mass of fragments made by GI is about half of Jupiter mass ([Boley et al. 2010](#)) if not more ([Forgan & Rice 2013](#)).

In contrast, here it was shown that TD naturally produces \sim Neptune mass planets in the relevant separation, time and mass ranges (see §5.4). Such planets do not accrete gas from the disc, at least not until their cores cool down, which is probably longer than the disc lifetime in most systems.

A planet mass nearer to Neptune mass would yield much longer migration time scales, closer to the expected age of HL Tau. The smaller planet mass would also be consistent with the \sim Neptune mass limits earlier obtained for the embedded HL Tau planets by [Tamayo et al. \(2015\)](#). This would not necessarily contradict [Dipierro et al. \(2015\)](#) results. Due to numerical constraints, their simulations were run for only $\sim 5,000$ years, which is much shorter than the likely HL Tau age. Neptune or somewhat smaller mass planets may well open sufficiently deep depressions in the dust distribution in simulations ran for longer and/or with lower artificial viscosity.

In appendix B, an even more distant massive core formation was demonstrated. TD hence can produce massive young cores orbiting the host star well beyond 100 AU. TD hence predicts that dust rings in discs even larger than those detected by ALMA in HL Tau may be common place in young protoplanetary discs.

6.5 Uranus, Neptune and the outer Solar System

Uranus and Neptune, located at $a \approx 19$ and 30 AU, respectively, have masses $M_{\text{p}} = 14.5$ and $17 M_{\oplus}$. Even for Uranus with its less distant location, [Pollack et al. \(1996\)](#) found core growth time of 16 Myr, which is too long to explain the presence of Hydrogen on that planet. More recent models find much higher solid accretion rates (e.g., [Lambrechts & Johansen 2012](#)), cutting the growth time for Uranus and Neptune’s cores significantly. However,

[Helled & Bodenheimer \(2014\)](#) show that for these higher accretion rates the issue is in understanding why these planets accreted just a little gas, e.g., why gas accretion stopped just before the runaway gas accretion phase commenced, and that formation of such planets in CA is still not trivial.

In the model presented here, massive cores of $\sim 10 - 15 M_{\oplus}$ with Hydrogen atmospheres of a few M_{\oplus} form quite frequently (see fig. 5). The special meaning of this mass range is explained rather naturally by eq. 2. The cores do not accrete more gas from the disc easily since their luminosity is significant.

As suggested earlier by [Handbury & Williams \(1975\)](#); [Nayakshin & Cha \(2012\)](#), the outer Solar System, including the Kuiper belt, may be rather naturally formed due to self-induced disruptions of two or more gas fragments of a Jupiter mass. More generally, here it was shown that self-disruption of planets at large distances makes debris discs with radii of tens and even hundreds of AU in the context of TD, as required to explain the observed large debris rings (e.g., [Wyatt 2008](#)).

6.6 Metal monster planets

Planets in general, and gas giant planets in particular, are over-abundant in metals compared to their host stars ([Saumon & Guillot 2004](#); [Miller & Fortney 2011](#)). In TD scenario, such over-abundance of metals arises from accretion of pebbles onto pre-collapse gas fragments (cf. §8 and fig. 17 in [Nayakshin & Fletcher 2015](#)). [Nayakshin \(2015b,c\)](#) argued that gas fragments accrete $\sim 10\%$ of their mass in pebbles before they collapse by H_2 dissociation.

Strong feedback by the core puffs the fragments up, hence requiring more pebble accretion for collapse. In §5.6 it was shown that the more massive the core is, the more metal rich the gas giant planet is, in general. In addition, a branch of even more highly metal-enriched planets was found, with metallicities Z_{pl} up to extreme values of ~ 0.5 (see the top panel of fig. 7). These “metal monsters” are rare in the current simulations (a few % of the survived gas giant population), and more detailed fragment and disc models are needed to nail down their expected frequency.

Nevertheless, it is interesting to note that there may already exist observational counterparts to the metal monsters. CoRoT-20b is a $M_{\text{p}} \approx 4.2 M_{\text{J}}$ gas giant that has been estimated to contain $\sim 800 M_{\oplus}$ (which is $\sim 60\%$ by weight!) of metals if they are all locked in the core, or perhaps ~ 300 to $400 M_{\oplus}$ if the metals are in the envelope ([Deleuil et al. 2012](#)). Its metal abundance is hence $0.25 \leq Z_{\text{pl}} \leq 0.6$. Furthermore, many of the strongly irradiated gas giant planets are inflated ([Miller & Fortney 2011](#)), but others are not. It is possible that those that are not inflated despite being irradiated by high fluxes contain more metals than assumed in the models. This implies that some of such non-inflated but very hot Jupiters may have very high metallicities.

6.7 Uncertainties and future work

The sources of uncertainties in this work come from several factors. First of all, it is desirable to model the internal evolution of the fragment better by using a fully fledged planet/stellar evolution code, as done, by, e.g.,

Vazan & Helled (2012). This may affect the maximum mass of the cores made inside the fragments. It is also desirable to model the "solid" core explicitly via the same stellar evolution code rather than via a constant density approximation to be able to calculate the energy release by the core better. This is a very difficult task at the moment since opacity and equation of state for hot super-Earth mass cores are not well understood yet (Stamenković et al. 2012).

Grain micro-physics is another worry. Three grain species are included here, but in reality there are many more, and there is a possibility that individual grains are composed of a number of different species.

Fragment-disc interactions are another source of model dependencies. In particular pebble accretion rates, are modelled in the "Hill's regime", e.g., when all pebbles (grains with Stock's number ~ 1) entering the Hill's sphere of the planet are accreted (Lambrechts & Johansen 2012). This may not be a good approximation if the planet itself is migrating rapidly through the disc. A 3D hydrodynamics study of this issue is required.

These and many other modelling uncertainties are clearly a worry. However, the critical self-disruption mass limit (eq. 2) is derived based on a simple energy argument, so it is hard to see how it may be *very* sensitive to these effects. Furthermore, another major set of results, the planet correlations with host metallicities (which were explored in great detail in Nayakshin & Fletcher 2015) are likely to be robust because they arise from "common sense" trends, such as higher pebble accretion rate onto the fragments in high metallicity protoplanetary discs, which are expected to hold in 1D or 3D simulations.

7 CONCLUSIONS

Here it was suggested that the role of massive cores in gas giant planet formation is not at all positive. By unleashing energetic feedback onto their host fragments in the first ~ 0.1 –1 Million years of their life, when the fragments are most vulnerable to stellar tides of the host star, massive cores ensure that they are the dominant population of planets. However, the cores are also victims of their own success: their mass cannot exceed ~ 10 –20 M_{\oplus} because their hosts cannot withstand stronger feedback by more massive cores, and get disrupted before the cores could grow more massive. There is a number of observational predictions that distinguish TD from CA scenario and hence I hope that these two theories will be observationally differentiated in a very near future.

ACKNOWLEDGEMENTS

Theoretical astrophysics research at the University of Leicester is supported by a STFC grant. This paper used the ALICE High Performance Computing Facility at the University of Leicester. The authors is thankful to the anonymous referee whose comments improved the paper significantly.

REFERENCES

Agertz O., Kravtsov A. V., Leitner S. N., Gnedin N. Y., 2013, *ApJ*, **770**, 25

- Andrews S. M., Williams J. P., 2005, *ApJ*, **631**, 1134
 Baruteau C., Meru F., Paardekooper S.-J., 2011, *MNRAS*, **416**, 1971
 Batalha N. M., et al., 2013, *ApJS*, **204**, 24
 Biller B. A., et al., 2013, *ApJ*, **777**, 160
 Bodenheimer P., 1974, *Icarus*, **23**, 319
 Boley A. C., Hayfield T., Mayer L., Durisen R. H., 2010, *Icarus*, **207**, 509
 Boss A. P., 1997, *Science*, **276**, 1836
 Bowler B. P., Liu M. C., Shkolnik E. L., Tamura M., 2015, *ApJS*, **216**, 7
 Cen R., Ostriker J. P., 1999, *ApJ*, **514**, 1
 Cha S.-H., Nayakshin S., 2011, *MNRAS*, **415**, 3319
 Clarke C. J., 2007, *MNRAS*, **376**, 1350
 Crida A., Morbidelli A., Masset F., 2006, *Icarus*, **181**, 587
 Dale J. E., Bonnell I. A., 2008, *MNRAS*, **391**, 2
 Deleuil M., et al., 2012, *A&A*, **538**, A145
 Dipierro G., Price D., Laibe G., Hirsh K., Cerioli A., Lodato G., 2015, ArXiv 1507.06719,
 Fall S. M., Rees M. J., 1985, *ApJ*, **298**, 18
 Fischer D. A., Valenti J., 2005, *ApJ*, **622**, 1102
 Forgan D., Rice K., 2013, *MNRAS*, **430**, 2082
 Guillot T., 2005, *Annual Review of Earth and Planetary Sciences*, **33**, 493
 Haisch Jr. K. E., Lada E. A., Lada C. J., 2001, *ApJ*, **553**, L153
 Handbury M. J., Williams I. P., 1975, *AP&SS*, **38**, 29
 Hayashi C., Nakazawa K., Nakagawa Y., 1985, in Black D. C., Matthews M. S., eds, *Protostars and Planets II*. pp 1100–1153
 Helled R., Bodenheimer P., 2011, *Icarus*, **211**, 939
 Helled R., Bodenheimer P., 2014, *ApJ*, **789**, 69
 Helled R., Schubert G., 2008, *Icarus*, **198**, 156
 Helled R., Podolak M., Kovetz A., 2008, *Icarus*, **195**, 863
 Helled R., et al., 2014, *Protostars and Planets VI*, University of Arizona Press, pp 643–665
 Hori Y., Ikoma M., 2011, *MNRAS*, **416**, 1419
 Howard A. W., et al., 2012, *ApJS*, **201**, 15
 Hubickyj O., Bodenheimer P., Lissauer J. J., 2005, *Icarus*, **179**, 415
 Ida S., Lin D. N. C., 2004, *ApJ*, **616**, 567
 Ikoma M., Nakazawa K., Emori H., 2000, *ApJ*, **537**, 1013
 Johansen A., Blum J., Tanaka H., Ormel C., Bizzarro M., Rickman H., 2014, *Protostars and Planets VI*, University of Arizona Press, Tucson, pp 547–570
 Kenyon S. J., Bromley B. C., 2015, preprint, (arXiv:1501.05659)
 King A., 2003, *ApJ*, **596**, L27
 King A., Pounds K., 2015, *ARA&A*, **53**, 115
 Kobayashi H., Tanaka H., Krivov A. V., 2011, *ApJ*, **738**, 35
 Krumholz M. R., Klein R. I., McKee C. F., Offner S. S. R., Cunningham A. J., 2009, *Science*, **323**, 754
 Kuiper G. P., 1951, *Proceedings of the National Academy of Science*, **37**, 1
 Lambrechts M., Johansen A., 2012, *A&A*, **544**, A32
 Lambrechts M., Johansen A., 2014, *A&A*, **572**, A107
 Larson R. B., 1969, *MNRAS*, **145**, 271
 Lodders K., 2003, *ApJ*, **591**, 1220
 Machida M. N., Inutsuka S.-i., Matsumoto T., 2011, *ApJ*, **729**, 42
 Marley M. S., Fortney J. J., Hubickyj O., Bodenheimer P., Lissauer J. J., 2007, *ApJ*, **655**, 541
 Mayor M., et al., 2011, ArXiv e-prints (astro-ph 1109.2497),
 Michael S., Durisen R. H., Boley A. C., 2011, *ApJ*, **737**, L42+
 Miller N., Fortney J. J., 2011, *ApJ*, **736**, L29
 Mizuno H., 1980, *Progress of Theoretical Physics*, **64**, 544
 Mordasini C., Alibert Y., Benz W., Naef D., 2009, *A&A*, **501**, 1161
 Mordasini C., Alibert Y., Benz W., Klahr H., Henning T., 2012, *A&A*, **541**, A97
 Nayakshin S., 2010a, *MNRAS*, **408**, L36

- Nayakshin S., 2010b, *MNRAS*, **408**, 2381
 Nayakshin S., 2011a, *MNRAS*, **410**, L1
 Nayakshin S., 2011b, *MNRAS*, **413**, 1462
 Nayakshin S., 2014, *MNRAS*, **441**, 1380
 Nayakshin S., 2015a, ArXiv e-prints (arxiv: 1411.5264),
 Nayakshin S., 2015b, *MNRAS*, **446**, 459
 Nayakshin S., 2015c, *MNRAS*, **448**, L25
 Nayakshin S., Cha S.-H., 2012, *MNRAS*, **423**, 2104
 Nayakshin S., Cha S.-H., 2013, *MNRAS*, **435**, 2099
 Nayakshin S., Fletcher M., 2015, *MNRAS*, **452**, 1654
 Nayakshin S., Helled R., Boley A. C., 2014, *MNRAS*, **440**, 3797
 Pollack J. B., Hubickyj O., Bodenheimer P., Lissauer J. J.,
 Podolak M., Greenzweig Y., 1996, *Icarus*, **124**, 62
 Rafikov R. R., 2006, *ApJ*, **648**, 666
 Rice W. K. M., Lodato G., Armitage P. J., 2005, *MNRAS*,
364, L56
 Rice K., Lopez E., Forgan D., Biller B., 2015, preprint,
 (arXiv:1508.06528)
 Safronov V. S., 1972, Evolution of the protoplanetary cloud and
 formation of the earth and planets.. Jerusalem (Israel): Israel
 Program for Scientific Translations, Keter Publishing House,
 212 p.
 Safronov V. S., 1978, *Icarus*, **33**, 3
 Saumon D., Guillot T., 2004, *ApJ*, **609**, 1170
 Shakura N. I., Sunyaev R. A., 1973, *A&A*, **24**, 337
 Silburt A., Gaidos E., Wu Y., 2015, *ApJ*, **799**, 180
 Silk J., Rees M. J., 1998, *A&A*, **331**, L1
 Stamenković V., Noack L., Breuer D., Spohn T., 2012, *ApJ*,
748, 41
 Stevenson D. J., 1982, *P&SS*, **30**, 755
 Sunyaev R. A., Zeldovich Y. B., 1972, *A&A*, **20**, 189
 Tamayo D., Triaud A. H. M. J., Menou K., Rein H., 2015,
 preprint, (arXiv:1502.05099)
 Tsukamoto Y., Takahashi S. Z., Machida M. N., Inutsuka S., 2015,
MNRAS, **446**, 1175
 Vassiliadis E., Wood P. R., 1993, *ApJ*, **413**, 641
 Vazan A., Helled R., 2012, *ApJ*, **756**, 90
 Vorobyov E. I., 2013, *A&A*, **552**, A129
 Vorobyov E. I., Basu S., 2006, *ApJ*, **650**, 956
 White S. D. M., Rees M. J., 1978, *MNRAS*, **183**, 341
 Wyatt M. C., 2008, *ARA&A*, **46**, 339

APPENDIX A: NUMERICAL METHODS

A1 Description of a single planet formation experiment

Each planet formation experiment presented here models the last stages of the protoplanetary disc evolution, in which the disc around a protostar of mass $M_* = 1M_\odot$ stops receiving mass from an external infalling gas envelope. During the simulations, the disc mass monotonically decreases due to accretion of gas onto the star and photo-evaporation of the disc material. The disc photo-evaporation prescription is the sum of internal and an external photo-evaporation terms (see below), normalised so that the mean disc lifetime is ~ 3 Million years, as observed (Haisch et al. 2001).

In parallel to this, the evolution of a gas fragment born in the disc at separation $a \sim 100$ AU is followed. The fragment exchanges angular momentum with the disc via gravitational torques and migrates inward. The simulation stops when either the fragment migrated all the way through the disc to the disc inner boundary at $R = R_{\text{in}}$, or both the disc and the fragment stop evolving. In the latter case, by the end of the simulation the disc is dissipated away and

the planet has either collapsed (became a gas giant planet) or was downsized to a smaller planet. Typically, the simulations span from a fraction of 1 Million year to a little over 10 Million years. A single run takes between a few hours to a few days on a single CPU. I use the University of Leicester and UK national super-computers to run tens of thousands of models (see Acknowledgement).

Although it is likely that a number of fragments are born in the self-gravitating protoplanetary disc, especially in the earlier more massive phase, only one fragment per disc is simulated at this time.

A2 Disc evolution model

The protoplanetary disc is treated in the 1D azimuthally symmetric approximation, on a logarithmic radial grid extending from radius $R_{\text{in}} = 0.08$ AU to $R_{\text{out}} = 400$ AU. The disc has an initial surface density profile $\Sigma_0(R) \propto (1/R)(1 - \sqrt{R_{\text{in}}/R}) \exp(-R/R_{\text{disc}})$, where $R_{\text{disc}} = 100$ AU is the disc radial length scale. The normalisation for $\Sigma_0(R)$ is set by specifying the total initial disc mass, M_d , integrated from R_{in} to R_{out} . To evolve the disc, the time-dependent standard accretion disc equations of Shakura & Sunyaev (1973) are solved. For the surface density equation, the additional torque of the planet on the disc and the disc photo-evaporation terms are included:

$$\frac{\partial \Sigma}{\partial t} = \frac{3}{R} \frac{\partial}{\partial R} \left[R^{1/2} \frac{\partial}{\partial R} (R^{1/2} \nu \Sigma) \right] - \frac{1}{R} \frac{\partial}{\partial R} (2\Omega R^2 \lambda \Sigma) - \dot{\Sigma}_{\text{ev}} \quad (\text{A1})$$

where $\Sigma(R)$ is the disc surface density, $\Omega(R) = \sqrt{GM_*/R^3}$ is the Keplerian angular frequency at radius R , viscosity $\nu = \alpha_{SSC} c_s H$, where c_s and H are the midplane sound speed and the disc height scale, $\lambda = \Lambda / (\Omega R)^2$, and Λ is the specific tidal torque from the planet, which switches from type I to type II prescription following the results of Crida et al. (2006). The expression for both type I and type II λ are standard [see Nayakshin (2015a)], but type I migration regime timescale is further multiplied by a factor $1 \leq f_{\text{migr}}$ as in Ida & Lin (2004).

The last term in equation A1 is the disc photo-evaporation rate, which is the sum of internal UV and X-ray terms (Nayakshin & Fletcher 2015), e.g., due to the host's star radiation, and an external irradiation term. The latter is given by expressions from Clarke (2007) multiplied by 0.01. Following Mordasini et al. (2012), we introduce a Monte Carlo random variable $0.02 < \zeta_{\text{ev}} < 3$, which is the photo-evaporation rate multiplier. The upper and lower limits to ζ_{ev} are found such as to fit the mean observed protoplanetary disc lifetime of ~ 3 Myr (Haisch et al. 2001).

The disc viscosity follows the classical Shakura & Sunyaev (1973) prescription, but with the coefficient $\alpha = \alpha_0 + \alpha_{\text{sg}}$, being a sum of a constant, α_0 , and the self-gravity term that depends on the local disc Toomre's parameter, Q :

$$\alpha_{\text{sg}} = 0.2 \frac{Q_0^2}{Q_0^2 + Q^2} \quad (\text{A2})$$

where Q is the local Toomre's parameter. The parameter Q_0 , setting the transition from a viscosity driven by gravito-turbulence (Rice et al. 2005) to the non self-gravitating one, is set to $Q_0 = 1.5$ here. α_0 is a Monte-Carlo variable (cf. Table S1).

Fig. B1 shows the disc fraction in our model (red) versus time for a sample of 3000 discs without planets. The black curves show $f_{\text{disc}0} = \exp(-t/\tau_{\text{disc}})$, with $\tau_{\text{disc}} = 3$ Myr. However, the age of a protostar may be uncertain by ~ 1 Myr. To take this uncertainty into account, we also consider $f_{\text{disc}1} = 1$ for $t < 1$ Myr, and $f_{\text{disc}1} = \exp(-t'/\tau_{\text{disc}})$, where $t' = t - 1$ Myr, to be a reasonable fit to the data. The simulated disc fraction dependence with time provides a reasonably close description of the data, falling in-between the two power-law lines ($f_{\text{disc}0}$ and $f_{\text{disc}1}$).

A3 Planet evolution module

The planet evolution module is nearly identical to that described in section 4 of Nayakshin (2015a), with changes listed in section 2.2.2 of Nayakshin & Fletcher (2015). In brief, the planet formation module calculates, in 1D spherically symmetric approximation, the evolution of the internal structure of a gas fragment of an initial mass M_0 with grains treated in a second-fluid approximation. Since gas accretion onto the fragment is assumed to be inefficient (Nayakshin & Cha 2013), the fragment has a fixed gas mass, $(1 - Z_0)M_0$, where Z_0 is the initial metallicity of the fragment and the surrounding protoplanetary disc. However, the fragment accretes grains by pebble accretion (Lambrechts & Johansen 2014) from the disc at the rate, \dot{M}_z , determined by the disc evolution module of the code. The pebbles are deposited in the outermost layers of the fragment. Due to this, the metallicity of the fragment, Z , increases with time. The grains are allowed to grow via grain sticking collisions and sediment towards the centre (Boss 1997; Helled et al. 2008). The internal structure of the core in the centre of the fragment is not modelled, assuming simply a sphere with a constant material density $\rho_0 = 3 \text{ g cm}^{-3}$.

The treatment of grains inside the gas fragment follows sections 4.2, 4.3, and 4.6 of Nayakshin (2015a). Three grain species – water, rocks and CHON – are followed. CHON is a material made of carbon, hydrogen, oxygen, and nitrogen, excluding water; the material properties and vapour pressure are taken to be similar to that of the grains in the coma of Comet Halley (Helled et al. 2008). The three species are in relative abundances of 0.5, 0.25 and 0.25, respectively. Grains grow by sticking collisions, although they fragment if they sediment at too high velocity (see below). Turbulence and convective grain mixing are also included, and oppose grain sedimentation. Grains vaporise once the temperature exceeds the vaporisation temperature for given species. Core assembly by grain sedimentation therefore depends sensitively on the temperature and convection in the inner regions of the gas fragment. Accretion of grains onto the core is modelled as in section 4.4 of Nayakshin (2015a).

Since the energy transport within the gas fragment is dominated by convection soon after its formation (Helled et al. 2008), I assume the fragments to be isentropic. For such a fragment, and a given equation of state (EOS), there exists a relation between the central temperature, T_c , and the total energy of the fragment, E_{tot} . At time $t = 0$, an initial value for T_c is specified. The hydrostatic balance equation for the fragment is solved to determine the initial E_{tot} and the fragment’s radius, R_p . The fragment’s luminosity is also determined at this step. E_{tot} is then evolved according to equation (2), and the procedure repeated again.

The equation of state for the gas includes molecular Hydrogen’s vibrational and rotational degrees of freedom, molecule dissociation, and Hydrogen atom ionisation at high temperatures. Latent heat of grain vaporisation is also included.

A4 Core growth and luminosity

Core growth via grain sedimentation in my model is indirectly controlled by two parameters – the turbulence parameter α_d and the breaking velocity v_{br} . The former sets the diffusive grain mixing by turbulence (Nayakshin 2015a), which opposes grain sedimentation. In Nayakshin & Fletcher (2015), the turbulent diffusion parameter α_d was a Monte Carlo variable with limits from 10^{-4} to 10^{-2} . For larger values of α_d in this range, turbulence slows down grain assembly significantly. In this paper we wish to study the limit of a rapid assembly of massive solid cores, thus we use a fixed value of $\alpha_d = 10^{-4}$. This is low enough to provide a minimal resistance to grain sedimentation via turbulent diffusion. Note that this does not affect the convective grain mixing, which still offers a significant impediment to grain sedimentation, especially once the core is luminous enough.

The breaking velocity of grains is set by their material properties. Collisions of grains with velocities $v < v_{\text{br}}$ are assumed sticking, leading to grain growth, whereas collisions with velocities exceeding v_{br} lead to grain fragmentation and hence decrease in the grain size. This limits average grain size to a few cm, typically. Breaking velocity is a Monte-Carlo variable, with upper and lower limits of 15 and 30 m s^{-1} (cf. Table S1).

Since the internal structure of the core is not explicitly modelled, the core’s luminosity cannot be calculated from first principles. The situation studied here – a rapid, e.g., $\sim 10^4$ to $\sim 10^5$ years, assembly of a core as massive as $10 M_{\oplus}$ inside a dense hot gas envelope – is significantly different from that envisaged by Safronov (1978) in CA theory. In the classical CA, the gas-free assembly of terrestrial planets was thought to take as long as $\sim 10^8$ years. In that case it is reasonable to assume that the accretion energy of grains or planetesimals falling onto the core is radiated away “immediately” (Safronov 1978). In the problem at hand, however, grain accretion energy is first deposited into exciting the internal degrees of freedom of molecules and atoms, e.g., ionization of upper loosely bound energy levels of atoms, and the general heating of the core. The energy will be eventually emitted by the core, of course, as the core cools and contracts, but a rigorous calculation of the rate of this process is beyond what is possible at the present.

I follow the approach of Nayakshin (2015a); Nayakshin & Fletcher (2015), in which L_{core} represents the delayed grain accretion luminosity of the core. The core emits its energy of accretion on a finite time scale, t_{kh} , where t_{kh} is free parameter of the model, the Kelvin-Helmholtz contraction time of the core:

$$L_{\text{core}} = \frac{E_{\text{core}}}{t_{\text{kh}}}, \quad (\text{A3})$$

where E_{core} is the residual potential energy of the core,

which is integrated in time according to

$$\frac{dE_{\text{core}}}{dt} = \frac{GM_{\text{core}}\dot{M}_c}{R_{\text{core}}} - \frac{E_{\text{core}}}{t_{\text{kh}}}. \quad (\text{A4})$$

M_{core} and R_{core} are the running (current) core’s mass and radius. These two equations implement a delayed release of total energy $GM_{\text{core}}/2R_{\text{core}}$ at $t = \infty$, in which case M_{core} and R_{core} are the final mass and radius of the core. In the limit of $t_{\text{kh}} \rightarrow 0$ the energy release described by equation A4 is given by the instantaneous accretion luminosity, as in the usual approach in the Core Accretion theory. For simulations ST, $t_{\text{kh}} = 3 \times 10^5$ years, whereas it is $t_{\text{kh}} = 3 \times 10^{10}$ years for runs DC.

A5 Population synthesis parameter range

To enact a statistically meaningful study, I define a number of Monte-Carlo variables with a lower and an upper limit (see Table S1). For each Monte-Carlo variable, the distribution is uniform in the log of the parameter, except for host star metallicity, and is distributed between the minimum and the maximum values given in Table 1. For example, the initial protoplanetary disc mass varies between $0.075M_{\odot}$ and $0.2M_{\odot}$, while the disc viscosity parameter is sandwiched between $5 \times 10^{-3} < \alpha_0 < 0.05$.

For the host star metallicity distribution, a Gaussian distribution is used,

$$\frac{dp(Z_L)}{dZ_L} = \frac{1}{\sigma(2\pi)^{1/2}} \exp\left[-\frac{Z_L^2}{2\sigma^2}\right] \quad (\text{A5})$$

where $Z_L = [\text{Fe}/\text{H}] = [\text{M}/\text{H}]$, the usual logarithmically defined metallicity, $\sigma = 0.22$, and dp/dZ_L is the probability density. $Z_L \equiv \log_{10}(Z/Z_{\odot})$, where $Z_{\odot} = 0.015$ is the Solar metallicity, that is, the fraction of mass in astrophysical metals compared to the total mass of the Sun. Obviously, $Z = Z_{\odot}10^{Z_L} = Z_{\odot}10^{[\text{M}/\text{H}]}$.

As explained in the main text, runs ST, DC and NC are each comprised of 3000 individual planet formation experiments. The run DC (“dim cores”) is different from ST only in that the Kelvin-Helmholtz time for the core is set to $t_{\text{kh}} = 3 \times 10^{10}$ years, rendering the cores too dim to affect the host fragment. In the simulation NC (“no cores”), core formation is artificially suppressed and grain growth disallowed.

APPENDIX B: SELF-DISRUPTION OF GAS FRAGMENTS AT $A > 100$ AU.

As pointed out in the main text, gravitational instability may be effective at distances well over 100 AU. For example, simulations of [Vorobyov & Basu \(2006\)](#) show fragment formation on scales of hundreds of AU. Here we show that fragments born by GI at distances greater than HL Tau rings may also form massive cores by self-disruption of the young low mass gas clumps. Figure S.2 shows how a gas fragment initialised at $a = 150$ AU evolves in our disc. Since the disc surface density is much lower at these distances, the fragment migrates in much slower than the fragments born at $a \lesssim 100$ AU do. Pebble accretion rates are also lower (note the decrease in pebble accretion “luminosity”, L_{peb} in panel e of fig. S.2), hence the core growth is slower.

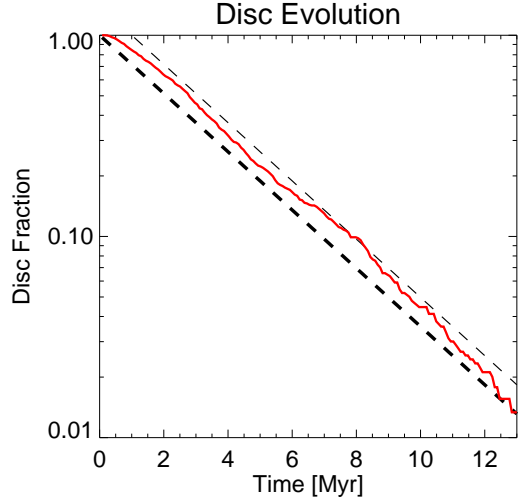


Figure B1. Simulated fraction of stars with discs as a function of time (red). The two power-law curves show approximate bounds within which the red line should fall to describe observational disc fraction dependence on the star’s age reasonably well.

Nevertheless, the end result is similar: the fragment is eventually disrupted at time $t \approx 0.8$ Myr, when the core mass reaches just above $5 M_{\oplus}$.

This paper has been typeset from a $\text{\TeX}/\text{\LaTeX}$ file prepared by the author.

Parameter	M_0	ζ_{ev}	f_p	a_0	M_d	f_{migr}	t_{kh}	α_d	v_{br}	α_0
Min	1/3	0.02	0.04	70	0.075	1	3×10^5	10^{-4}	15	5×10^{-3}
Max	8	3.0	0.08	105	0.2	4	3×10^5	10^{-4}	30	5×10^{-2}

Table B1. The range of the Monte Carlo parameters of the “standard” population synthesis calculation (run ST) for this paper. The first row gives parameter names, the next two their minimum and maximum values. The columns are: planet’s initial mass, M_0 , in Jupiter masses; ζ_{ev} , the evaporation rate factor; f_p , the pebble mass fraction determining the fraction of the disc grain mass in pebbles; a_0 [AU], the initial position of the fragment; M_d , the initial mass of the disc, in units of M_\odot ; f_{migr} , the type I planet migration factor; t_{kh} , in years, determines the luminosity of the core; α_d , turbulence parameter within the fragment; v_{br} , the grain breaking velocity, in m/s; the disc viscosity parameter, α_0 .

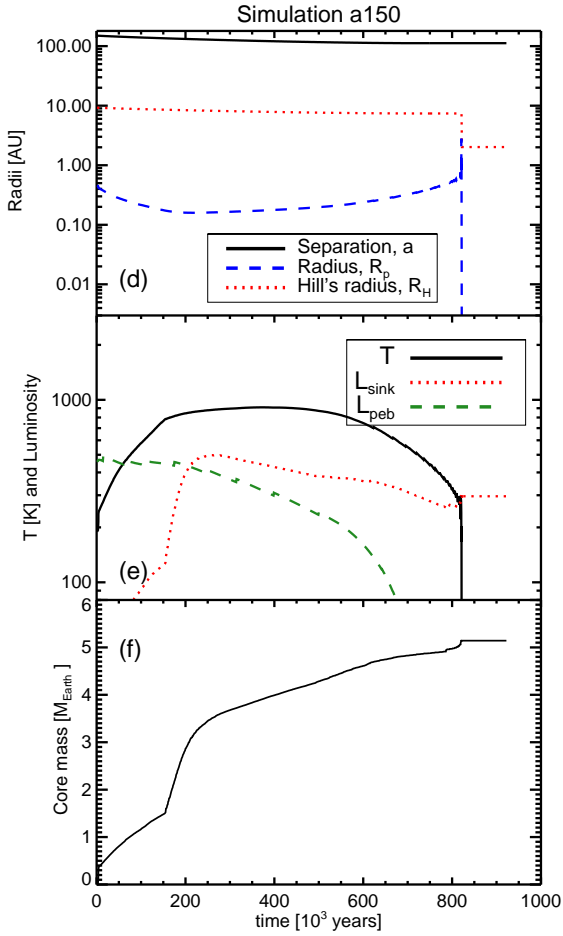


Figure B2. Simulation performed with same physics as the ST series of runs but with the fragment started at $a = 150$ AU. The fragment self-destructs and deposits the core of mass $\approx 5 M_\oplus$ back into the disc at $a = 112$ AU, where it remains.